Physicochem. Probl. Miner. Process., 62(3), 2026, 224759

http://www.journalssystem.com/ppmp

Physicochemical Problems of Mineral Processing

ISSN 1643-1049

Superiority of Cr- or Ti-implanted ZnS nanocrystal for ion adsorption: Structural-electronic analysis by DFT calculation

Fatemeh Mollaamin

Department of Biomedical Engineering, Faculty of Engineering and Architecture, Kastamonu University, Kastamonu, Turkey

Corresponding author: fmollaamin@kastamonu.edu.tr

Abstract: A detailed study was performed using "DFT" calculations at the "CAM-B3LYP-D3/6-311+G (d,p)" level to investigate how H_2O is captured by a ZnS, ZnTiS or ZnCrS heterocluster. The weak signal strength observed near the parallel edge of the nanocluster sample could be because of the non-spherical arrangement of the ZnS, ZnTiS or ZnCrS heterocluster caused by H/OH binding. This hypothesis about energy absorption was supported by analyzing the density distributions of "TDOS, PDOS, OPDOS, ESP" for both the bare and water-coated ZnS, ZnTiS and ZnCrS heteroclusters. An isosurface map showed a larger area involved in H_2O adsorption on the ZnS, ZnTiS or ZnCrS surface, leading to the formation of a hydrated ZnS (H^+OH^-), ZnTiS(H^+OH^-) and ZnCrS (H^+OH^-)complexes, with specific atoms labeled as "O1, Zn15/Ti15/Cr15, O27, H29, and H30". Based on this, it could be said that the Zn/Ti/Cr in the cubic ZnS, ZnTiS or ZnCrS, respectively has a greater ability to accept electrons during H_2O adsorption. It's also important to note that when all the surface elements of ZnS, ZnTiS or ZnCrS are covered by "OH^-/H^+" ions, the semiconducting treatment is restored. These findings suggest that the electronic properties can be adjusted by controlling the adsorption position on the ZnS, ZnTiS or ZnCrS surface. This study aims to explore methods for treating water and enhancing the effectiveness of titanium zinc sulfide and chromium zinc sulfide alloy photocatalysts in removing pollutants. The findings can potentially lead to the development of more efficient water purification processes through further research on photocatalysts.

Keywords: ZnTiS, ZnCrS, semiconducting heterocluster, H_2O-adsorption; first-principles study

1. Introduction

Zinc sulfide in its cubic form, known as ZnS, is the standard example of II–VI semiconductors. It has the smallest lattice constant (a_0), which is about 5.4102 angstroms at 300 K. This material is mostly used in devices that emit ultraviolet light because it has a wide "band-gap energy" at room temperature (Wang et al., 2015).

Many research teams have tried adding ions into the structure of zinc oxide or zinc sulfide, which helps in developing diverse complex applications because this changes their electronic properties and characteristics a lot. The improved catalytic abilities show how zinc oxide or zinc sulfide nanoparticles work together, which makes the "electron-hole" pairs more effective, leading to better catalytic performance when light is in the visible range. Importantly, the zinc oxide-based zinc sulfide nanocomposite was made using a wet chemical method without needing any templates. The sample approach is not very sensitive to the states used, is simple to do, and allows control over the structure, shape, and size of the nanomaterials through the template. In general, the excellent photocatalytic performance of wurtzite zinc oxide and zinc sulfide semiconductors, as well as their composites, under visible light is because they work well together when combined with other metal oxide semiconductors. This investigation is part of our ongoing work to explore directions related to solar energy conversion and harvesting. We have reported a simple way to make zinc sulfide and zinc oxide nanostructures and their nanocomposites using the wet chemical approach (Khan et al., 2022; Zagorac et al., 2022; De Moraes et al., 2021; Bolatov et al., 2024; Dong et al., 2018).

DOI: 10.37190/ppmp/224759

Additionally, "molecular dynamics simulations" of H_2O-adsorption on three and five nanometer sphalerite nanostructures helped explain how water attaches to these particles and how it interacts at the atomic level. The simulations also show that as the particle size gets smaller, the energy needed to bind water increases. This is because the water molecules on very small, curved surfaces are farther apart and interact less strongly with each other (Zhang et al., 2007).

The researchers did the detailed computer simulations to study how about 30 small molecules, which are parts of biomolecules, attach to zinc sulfide surfaces in water. They discovered that only a few negatively charged molecules, like the side chains of aspartic and glutamic acids, and the negative form of cysteine, stick strongly to the clean zinc sulfide surface. Most other molecules don't bind well or not at all. When zinc sulfide is in the form of round nanoparticles, these molecules bind more strongly because they attach at the edges where different parts of the surface meet. However, when the zinc sulfide is covered with PMMA, the way these molecules attach changes a lot (Rahmani and Lyubartsev, 2023).

A recent study looked into how well indium-doped ZnS nanopowders can produce hydrogen through photocatalytic reactions. These nanopowders were made using a method called microwave-assisted heating, which is fast and efficient. The nanopowders can directly use stream water for the water-splitting process. The study found that using more ZnS material leads to larger particles, but adding indium makes the particles smaller, increases the surface area, and greatly improves the rate at which hydrogen is produced (Chang et al., 2025).

ZnS nanoparticles have a high surface area compared to their size, resulting in a larger band gap. This characteristic makes them more suitable for emitting light through photoluminescence (Bhargava et al., 1994).

Doping can be used to create ZnS nanoparticles with different chemical and physical characteristics. This is crucial for producing semiconductor nanocrystals that are utilized in the production and commercialization of nanoscale devices. Dopants introduce impurity centers that interact with electrons and holes. As a result, numerous researchers have endeavored to create semiconductor nanostructures doped with transition metals (Choi et al., 2005; Radovanovic et al., 2005; Yatsunenko et al., 2008).

ZnS has a large band gap of 3.6 eV, which indicates that it can only absorb light in the ultraviolet range. However, it is easy to modify the amount of light it absorbs by introducing specific metal ions, such as Mn, Ni, Cu, or Pb (Kudo and Sekizawa, 2000).

Recently, researchers have investigated the use of ZnS nanostructure layers for photocatalytic water splitting, incorporating specific transition metal dopants and graphene as a decorator to enhance the efficiency of the water splitting process (Kiptarus et al., 2024).

Additionally, the density functional theory (DFT) approach included in the Quantum ESPRESSO software should be used to study the structural, electronic, and optical characteristics, as well as the chemical stability, of certain transition metal-doped ZnS nanosheet layers (Chaurasiya and Dixit, 2019). Chen et al. observed ferromagnetism in TM-doped ZnS by density functional theory (DFT) studies. They demonstrated that the Fe and Ni endohedral bi-doped $(ZnS)_{12}$ clusters favor the ferromagnetic state, which has potential applications in nanoscale quantum devices (Chen et al., 2011).

The researchers reported a theoretical study on the structural and electronic properties of the anatase phase of titanium dioxide (TiO_2) within the framework of density functional theory. Their results revealed that, after the zinc doping, the structure didn't change but there was a little expansion in the volume of the pure material. It was found that the doped structure's stability increases as the concentration of the dopant increases, but all the doped structures are stable (Alhassan et al., 2024).

In another research, the surface, size and ion doping effects on the magnetic, phonon and optical properties of ZnS nanoparticles are studied based on the s-d model including spin-phonon and Coulomb interaction and using a Green's function theory. The changes of the properties are explained on a microscopic level, due to the different radii between the doping and host ions, which cause different strains-compressive or tensile, and change the exchange interaction constants in our model. Band gap changes in doped semiconductors could be due because of exchange, s-d, Coulomb and electron-phonon interactions (Apostolova et al., 2023).

In this study, we looked at how H_2O adsorption affects the properties of a ZnS, ZnTiS or ZnCrS nanocluster. We used DFT calculations to examine the density of states, charge distribution, bond

orders, and HOMO-LUMO orbitals. The optimized structure of ZnS, ZnTiS or ZnCrS is shown in Fig. 1, and the zinc/titanium/chromium, oxygen and hydrogen atoms are labeled to help explain the reaction pathway.

In this study, the ZnS (H^+OH^-), ZnTiS (H^+OH^-), or ZnCrS (H^+OH^-) sensor was successfully used to detect relative humidity through nearest neighbor analysis. The way water molecules attach to the surfaces of ZnS, ZnTiS, or ZnCrS was also studied using density functional theory.

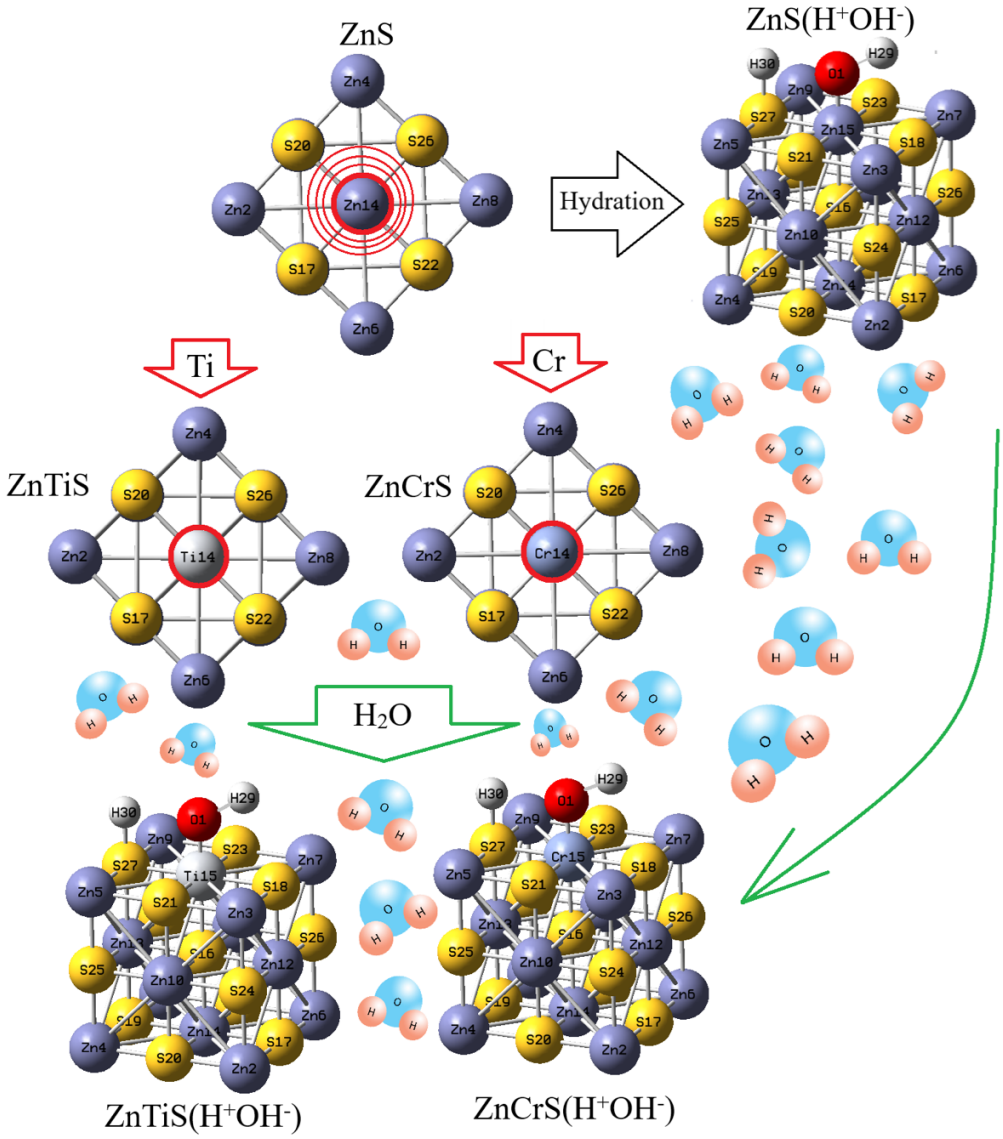

Fig. 1. Functionalization of pristine ZnS, alloys of ZnTiS, ZnCrS and hydrated complexes of ZnS (H^+OH^-), ZnTiS(H^+OH^-) and ZnCrS (H^+OH^-) complexes using a labeled ring showing H, O, Zn, Ti, Cr atoms involved in H_2O adsorption

2. Compounds, theory and methods

Improvement of the applied Density Functional Theory (DFT) methodology only became notable after W. Kohn and L. J. Sham released their reputable series of equations which are introduced as Kohn-Sham (KS) equations (Khon and Sham, 1965):

$$\hat{H}_s = -\sum_i^M \frac{1}{2} \bar{\nabla}_i^2 + \sum_i^M v_s(\vec{r}_i) = \sum_i^M \hat{h}_s \quad (1)$$

$$\hat{h}_s = -\frac{1}{2} \bar{\nabla}_i^2 + v_s(\vec{r}_i) \quad (2)$$

By representing the single particle orbitals ψ_i all electronic densities physically acceptable for the system of "non-interacting" electrons are written in the equation (3):

$$\rho\ (\vec{r}) = \sum_i^M |\psi_i\ (\vec{r})|^2 \quad (3)$$

Finally, the total energy could be measured by the KS method due to the equation (4):

$$E[\rho] = T_s[\rho] + \int dr\ \ v_{ext}\ (r)\rho(r) + E_{\mathrm{H}}[\rho] + E_{\mathrm{xc}}[\rho] \quad (4)$$

where kinetic energy functional, v_{ext} declares external potential, E_{H} is the "Hartree or Coulomb" energy and E_{xc} indicates exchange-correlation functional. Therefore, the precise exchange energy functional is described by the Kohn–Sham orbitals in lieu of the density which is cited as the indirect density functional. This research has employed the penetration of the hybrid functional of three-parameter basis set of B3LYP (Becke, Lee, Yang, Parr)" within the conception of DFT upon theoretical computations (Becke, 1993). The popular B3LYP (Becke, three-parameter, Lee–Yang–Parr) and exchange-correlation functional becomes based on equation (5) (Lee et al., 1988):

$$E_{\mathrm{XC}}^{\mathrm{B3LYP}} = (1-\alpha)E_{\mathrm{x}}^{\mathrm{LSDA}} + \alpha E_{\mathrm{x}}^{\mathrm{HF}} + b\Delta E_{\mathrm{x}}^{\mathrm{B}} + (1-c)E_{\mathrm{c}}^{\mathrm{LSDA}} + cE_{\mathrm{c}}^{\mathrm{LYP}} \quad (5)$$

Calculations with spin polarization were performed within the "density functional theory (DFT)".

The hydration of bare ZnS, ZnTiS or ZnCrS heterocluster and the formation of the hydrated " ZnS (H^+OH^-), ZnTiS (H^+OH^-) or ZnCrS (H^+OH^-)" heterocluster were studied using quantum mechanics computations based on "density functional theory (DFT)" (Fig. 1) (Mollaamin and Monajjemi, 2023a; Mollaamin and Monajjemi, 2023b). A "rigid potential energy surface" was calculated using "DFT" (Mollaamin, 2014) with the "Gaussian 16 revision C.01 program package" (Frisch et al., 2016) and "GaussView 6.1" (Dennington et al., 2016). The calculations used the "6-311+G(d,p)" basis set for energy storage applications in solar cells.

The structural settings of the ZnS, ZnTiS or ZnCrS heterocluster and the hydrated nanocluster of ZnS (H^+OH^-), ZnTiS (H^+OH^-) or ZnCrS (H^+OH^-), respectively, were adjusted to achieve the highest possible "short-circuit" current density. Fig. 1 shows how water molecules attach to the ZnS, ZnTiS or ZnCrS surface, and this process is modified to improve light absorption in the active area. This tool is applied to calculate the position and perimeter of a ring, as ring area is often considered in "wavefunction analysis". To use this function, you must enter the indices of the elements that form the ring in a clockwise order. This helps determine the total position and perimeter of a specific ring, which are 9.4242 Å and 12.2796 Å² for ZnS, respectively (Fig. 1).

3. Results and Discussion

In this article, the data assesses how effective ZnS, ZnTiS or ZnCrS heterocluster is in water using information about energy, shape, and charge obtained from "density functional theory" computations. The sample used matches well with quantum mechanics data for the hydrated ZnS (H^+OH^-), ZnTiS (H^+OH^-), ZnCrS or ZnCrS (H^+OH^-) system found in the "dataset". The force-field approach was used to examine how water molecules attach to the surface of ZnS, ZnTiS or ZnCrS at a single layer coverage.

3.1. Charge density distribution

Additionally, the atomic charge was examined during the adsorption of H_2O on ZnS, ZnTiS or ZnCrS nanocluster, which contributed to the formation of ZnS (H^+OH^-), ZnTiS (H^+OH^-), ZnCrS or ZnCrS (H^+OH^-) complex (Table 1).

The atomic charges of "zinc, titanium, chromium, oxygen, and hydrogen or hydroxyl groups" attached to ZnS, ZnTiS or ZnCrS have been measured. These measurements show that when water is added, the negative charge on oxygen atoms in the "O16 to O28" region of "hydrated ZnS, ZnTiS or ZnCrS " changes due to the coating of " ZnS, ZnTiS or ZnCrS with H or OH" groups. In fact, hydrated ZnS, ZnTiS or ZnCrS is more effective than pure ZnS, ZnTiS or ZnCrS at accepting electrons from the electron donor between O16 and O28 (Table 1 and Fig. 2). Water mainly attaches to the surface of ZnS, ZnTiS or ZnCrS nanoparticles by forming Zn-O, Ti-O, Cr-O bond. Compared to bulk ZnS crystals, ZnTiS or ZnCrS nanoparticles can hold more water molecules per unit surface area because their curved structure increases the distance between neighboring water molecules.

The analysis of charge density changes during the adsorption process shows that bare zinc sulfide and hydrated zinc sulfide nanoclusters have a "Bader charge" of "–1.747 and –1.900 " coulombs, respectively. The difference in charge density between these nanostructures is measured as $\Delta Q_{ads,\,ZnS}$ = –0.153 coulombs.

Moreover, ZnTiS / ZnTiS (H^+OH^-) and ZnCrS / ZnCrS (H^+OH^-) have shown the "Bader charge" of –1.856/–1.951 coulombs and –1.750/–1.931 coulombs for bare and hydrated complexes, respectively. Therefore, the difference in charge density between these nanostructures will be $\Delta Q_{ads,\ ZnTiS}$ = –0.095 coulombs and $\Delta Q_{ads,\ ZnCrS}$ = –0.181 coulombs. The results indicated that chromium ions can successfully replace zinc ions causing strong ferromagnetic behavior.

Table 1. The "atomic charge (Q/coulomb)" for "heteroclusters of bare ZnS, ZnS (H^+OH^-), ZnTiS, ZnTiS (H^+OH), ZnCrS and ZnCrS (H^+OH^-) (A – Atom, Ch – Charge)

ZnS		ZnS (H^+OH^-)		ZnTiS		ZnTiS (H^+OH^-)		ZnCrS		ZnCrS (H^+OH^-)	
A	Ch	A	Ch	A	Ch	A	Ch	A	Ch	A	Ch
Zn1	-0.5916	O1	-0.6526	Zn1	-0.492	O1	-0.1809	Zn1	-0.3426	O1	-0.2816
Zn2	-0.5915	Zn2	-0.5742	Zn2	-0.3587	Zn2	-0.5507	Zn2	-0.3882	Zn2	-0.4052
Zn3	-0.5915	Zn3	-0.5431	Zn3	-0.4919	Zn3	-0.1248	Zn3	-0.3425	Zn3	-0.2492
Zn4	-0.5914	Zn4	-0.5535	Zn4	-0.3586	Zn4	-0.558	Zn4	-0.388	Zn4	-0.3843
Zn5	-0.5914	Zn5	-0.4722	Zn5	-0.4916	Zn5	-0.033	Zn5	-0.3423	Zn5	-0.0665
Zn6	-0.5913	Zn6	-0.5761	Zn6	-0.3585	Zn6	-0.5502	Zn6	-0.3878	Zn6	-0.4049
Zn7	-0.5913	Zn7	-0.5656	Zn7	-0.4916	Zn7	-0.1165	Zn7	-0.3421	Zn7	-0.2633
Zn8	-0.5912	Zn8	-0.5528	Zn8	-0.3584	Zn8	-0.5605	Zn8	-0.3877	Zn8	-0.3891
Zn9	-0.4176	Zn9	-0.4722	Zn9	-0.7058	Zn9	-0.0439	Zn9	-0.2611	Zn9	-0.076
Zn10	-0.4179	Zn10	-0.4578	Zn10	-0.7062	Zn10	-0.7348	Zn10	-0.2617	Zn10	-0.3914
Zn11	-0.4175	Zn11	-0.4581	Zn11	-0.254	Zn11	-0.7358	Zn11	-0.2608	Zn11	-0.3768
Zn12	-0.4176	Zn12	-0.4646	Zn12	-0.2542	Zn12	-0.4694	Zn12	-0.261	Zn12	-0.4141
Zn13	-0.4175	Zn13	-0.5131	Zn13	-0.645	Zn13	-0.4638	Zn13	-0.483	Zn13	-0.5622
Zn14	-0.4176	Zn14	-0.3469	Ti14	-1.471	Zn14	0.0618	Cr14	-1.7726	Zn14	-0.0458
S15	0.6704	Zn15	-2.667	S15	0.7036	Ti15	-3.4773	S15	0.601	Cr15	-3.2443
S16	0.5475	S16	0.7342	S16	0.6886	S16	1.043	S16	0.5785	S16	0.613
S17	0.5473	S17	0.6123	S17	0.3793	S17	0.6833	S17	0.3087	S17	0.5992
S18	0.5473	S18	0.7932	S18	0.6885	S18	0.5213	S18	0.5783	S18	0.3666
S19	0.5475	S19	0.8517	S19	0.6819	S19	0.8101	S19	0.5785	S19	0.79
S20	0.5473	S20	0.5726	S20	0.5478	S20	0.6836	S20	0.3086	S20	0.5733
S21	0.5471	S21	1.1263	S21	0.6813	S21	0.4874	S21	0.5779	S21	0.5908
S22	0.5469	S22	0.5741	S22	0.5481	S22	0.6814	S22	0.3081	S22	0.5734
S23	0.5475	S23	1.1166	S23	0.5351	S23	0.4893	S23	0.5186	S23	0.5904
S24	0.5473	S24	0.5695	S24	0.5349	S24	0.524	S24	0.5184	S24	0.5144
S25	0.5471	S25	0.6185	S25	0.5346	S25	0.5499	S25	0.5181	S25	0.5448
S26	0.5471	S26	0.5693	S26	0.3792	S26	0.5242	S26	0.3085	S26	0.5126
S27	0.5469	S27	0.2986	S27	0.5345	S27	0.2303	S27	0.5179	S27	-0.064
---	---	S28	0.6184	---	---	S28	0.5451	---	---	S28	0.5429
---	---	H29	0.4588	---	---	H29	0.1083	---	---	H29	0.4509
---	---	H30	0.3556	---	---	H30	0.2947	---	---	H30	0.3568

Fig. 2. The change in "atomic charge (Q/coulomb)" for a) ZnS/ZnS (H^+OH^-), b) ZnTiS/ZnTiS(H^+OH^-), and c) ZnCrS/ZnCrS (H^+OH^-)"

3.2. Total density of states

To better understand the different adsorption behaviors of bare heteroclusters of " ZnS, ZnTiS, ZnCrS " and hydrated complexes of " ZnS (H^+OH^-), ZnTiS (H^+OH^-) and ZnCrS (H^+OH^-)", "total density of states (TDOS)" (Xu et al., 2024) was calculated using the Multiwfn program (Lu and Chen, 2012; Lu, 2024).

This parameter helps identify "significant chemical interactions", often occurring on the "convex side" (Fig. 3a, a', b, b', c, c'). Therefore, the original total "DOS (TDOS)" of the "isolated system" can be expressed as (Xu et al., 2024):

$$TDOS\ (E) = \sum_i \delta\ (E - \epsilon_i\ ) \tag{6}$$

$$G(x) = \frac{1}{c\sqrt{2\pi}} e^{-\frac{x^2}{2c^2}} \quad \text{where} \quad c = \frac{\text{FWHM}}{2\sqrt{2\ln x}} \tag{7}$$

In addition, the curve map of "broadened partial DOS (PDOS)" and overlap "DOS (OPDOS)" is useful for visualizing the "orbital composition" analysis, and the "PDOS function of fragment" "A" is defined as:

$$PDOS_A\ (E) = \sum_i \Xi_{i,A}\ F\ (E - \epsilon_i\ ) \tag{8}$$

where " $\Xi_{i,A}$" is the "composition of fragment" "A" in orbital "i". The OPDOS between fragment "A" and "B" is defined as:

$$OPDOS_{A,B}\ (E) = \sum_i \mathrm{X}_{A,B}^{i}\ F\ (E - \epsilon_i\ ) \tag{9}$$

where "$\mathrm{X}_{A,B}^{i}$" describes "the total cross term between fragments" "A" and "B" in orbital "i ". In the "TDOS map", "each vertical line" declares a "molecular orbital (MO) ", and the "dashed line" shows the position

of the "HOMO". The curve shows the "TDOS" computed based on the energy distribution of the molecular orbitals. Our findings suggest that electronic properties can be tailored by adjusting the "surface adsorption sites". In the positive energy range, the area between 0.1 to 0.2 a.u. shows a significantly higher state density compared to other regions for bare heteroclusters of " ZnS, ZnTiS, ZnCrS " and hydrated complexes of " ZnS (H^+OH^-), ZnTiS (H^+OH^-) and ZnCrS (H^+OH^-)" (Fig. 3a, a', b, b', c, c').

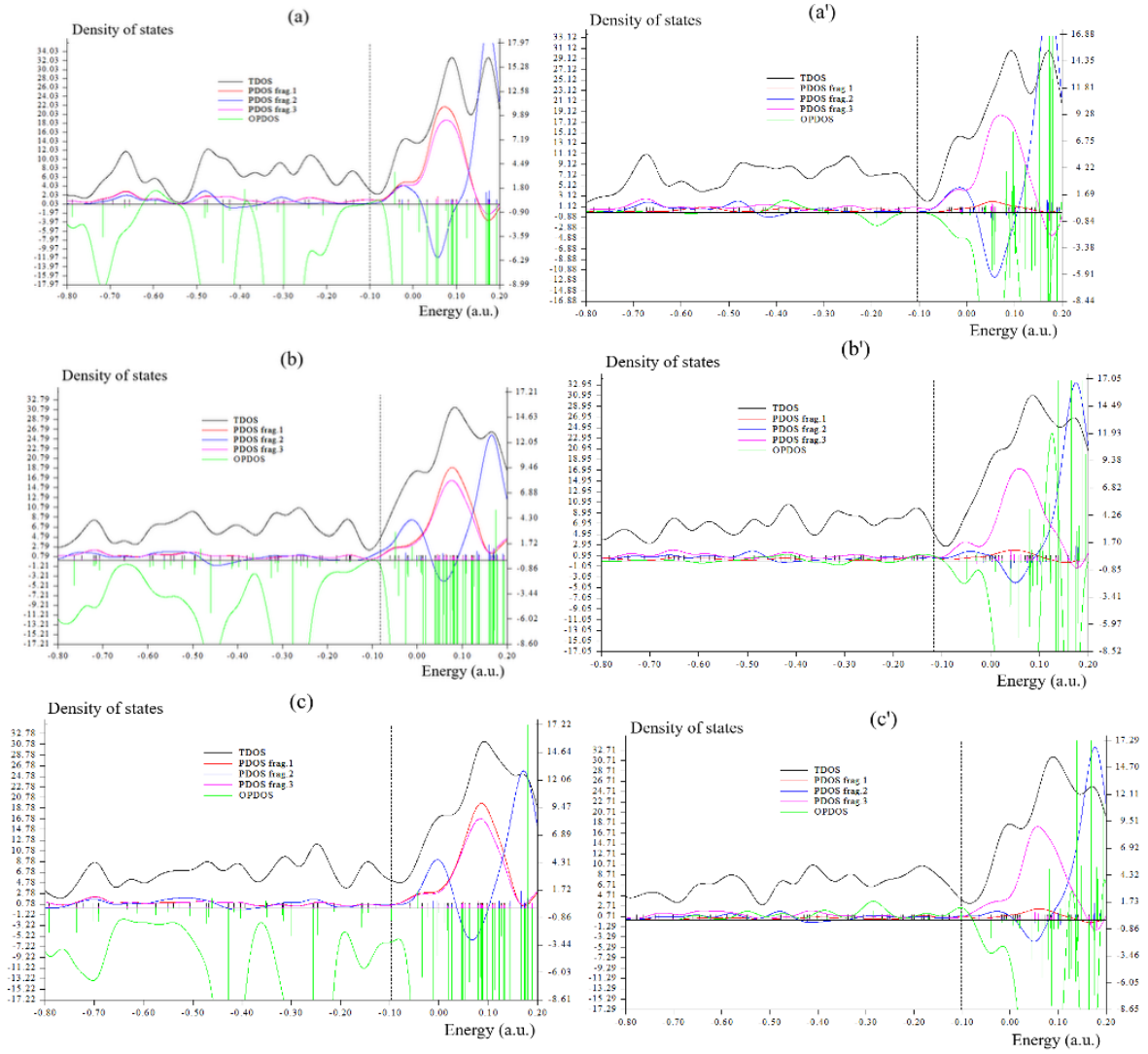

Fig. 3. The "TDOS/PDOS/OPDOS" graphs for heteroclusters of (a) bare ZnS, (a') ZnS (H^+OH^-), (b) ZnTiS, (b') ZnTiS (H^+OH^-), (c) ZnCrS and (c') ZnCrS (H^+OH^-).

Fragment 1 includes Zn1 (Fig. 3a), O1 (Fig. 3a'), and Zn2, Zn4, Zn6, Zn8, Zn10, O16, O19, O22, O24 (Fig. 3a, a') along with H30 (Fig. 3a'). Fragment 2 shows the movement of Zn11, Zn12, Zn13, Zn14, O17, O25, O26, O27 for both bare and hydrated ZnS, ZnTiS or ZnCrS heterocluster (Fig. 3b, b') and H29 specifically for hydrated ZnS, ZnTiS or ZnCrS heterocluster (Fig. 3b'). Fragment 3 includes the movement of O15 (Fig. 3c), Zn15/Ti15/Cr15 (Fig. 3c'), and "Zn3, Zn5, Zn7, Zn9, O18, O20, O21, O23" for both bare and hydrated ZnS, ZnTiS or ZnCrS heterocluster (Fig. 3c, c'). To show how each electron orbital contributes to the energy band, we have displayed the pure ZnO density of states (DOS) along with the partial density of states (PDOS) for both zinc and oxygen in panel c of Fig. 3. The DOS and PDOS graphs cover an energy range from -0.8 a.u. to 0.2 a.u., with the Fermi level set at 0 a.u.. The calculated band gap value of 3.401 eV is shown in the DOS plot. The two regions of the valence band, from -0.8 a.u. to -0.7 a.u. and from -0.7 a.u. to -0.6 a.u., are mainly contributed by the O(p) state and Zn(d) state, respectively. The energy band at the bottom of the conduction band is mainly made up of the Zn(4p) state, with a significant transition between the Zn(4p) and O(2p) states.

3.3. Molecular electrostatic potential (ESP) analysis

The molecular electrostatic potential (ESP) has been widely used for predicting the locations of nucleophilic and electrophilic reactions for a long time. It is also helpful in studying hydrogen bonds, halogen bonds, molecular recognition, and the interactions of aromatic molecules with each other (Murray et al., 2024). This function measures the electrostatic interaction between a single point charge placed at a position r and the molecule under study. A positive value indicates that the area is mainly influenced by nuclear charges, while a negative value indicates that it is more affected by electronic charges.

$$V_{tot}(r) = V_{nuc}(r) + V_{ele}(r) = \sum_A \frac{Z_A}{|r - R_A|} - \int \frac{\rho(r')}{|r - r'|} dr' \quad (10)$$

Z_A stands for the nuclear charge. If you are using a pseudopotential, then Z_A represents the number of electrons that are explicitly included. It is important to note that calculating the electrostatic potential (ESP) takes much more time compared to calculating other types of functions. Additionally, in Multiwfn, ESP is calculated exactly using nuclear attractive integrals, not through approximate methods like multipole expansion or solving the numerical Poisson equation. Due to this, the ESP results from Multiwfn may differ from those produced by other quantum chemistry software. To speed up the ESP calculation, Multiwfn skips some integrals that have minimal impact on the final result. The cutoff value for which integrals are skipped is set in the "espprecutoff" parameter in settings.ini. Increasing this value enhances the accuracy of the ESP but also increases the computational cost. In most scenarios, the ESP calculated with the default settings is accurate enough.

The heteroclusters made of bare and hydrated ZnS, ZnTiS or ZnCrS heteroclusters can be identified using ESP graphs, as they help in understanding the delocalization and localization of "electrons and chemical bonds" (Fig. 4 a, a', b, b', c, c').

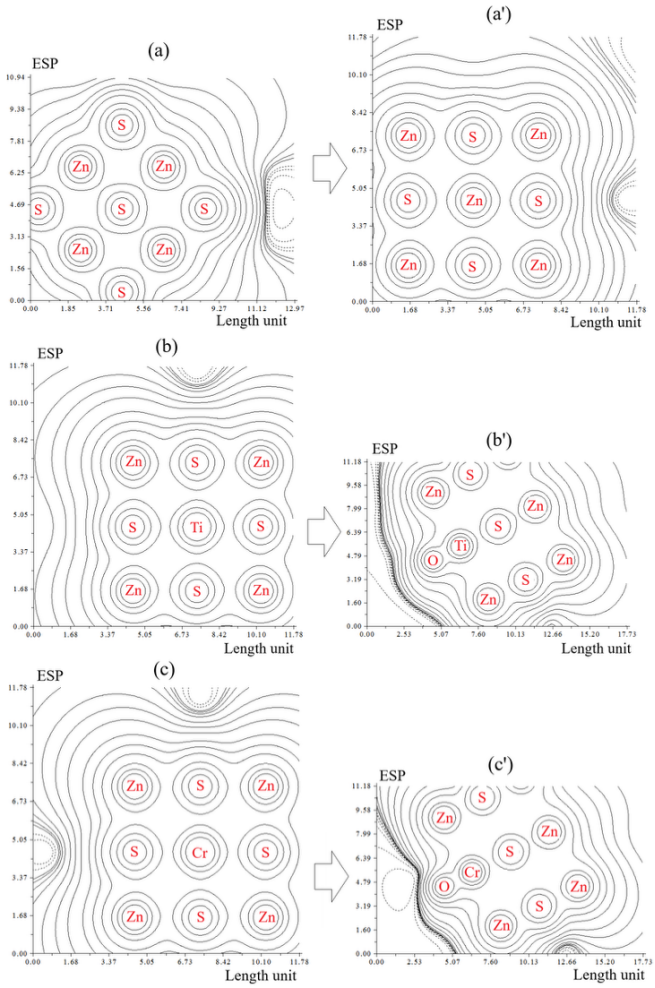

Fig. 4. Counter map graphs of the molecular electrostatic potential (ESP) for heteroclusters of (a) bare ZnS, (a') ZnS (H^+OH^-), (b) ZnTiS, (b') ZnTiS (H^+OH^-), (c) ZnCrS and (c') ZnCrS (H^+OH^-), plotted against length unit in Bohr.

"Covalent zones" have a "high ESP value", and the areas where electrons are missing between the "valence shell" and the inner shell are shown by the "blue circles around the nuclei" (Fig. 4a, a', b, b', c, c'). The shaded map of ESP for bare and hydrated ZnS, ZnTiS or ZnCrS heteroclusters (Fig. 4a, a', b, b', c, c') shows how the "localized orbital locator" changes with "H/OH adsorption". The hydrated heterocluster of ZnS (H^+OH^-), ZnTiS (H^+OH^-) or ZnCrS (H^+OH^-)" has a larger "isosurface map" of the "localized orbital locator" because it labels specific atoms like "O1, Zn15/Ti15/Cr15, O27, H29, and H30". A narrower connected area in the "isosurface map" suggests that the "localized orbital locator" is harder to achieve. However, the bigger "counter map" of ESP for hydrated heterocluster of ZnS (H^+OH^-), ZnTiS (H^+OH^-) or ZnCrS (H^+OH^-)" shows that ZnS, ZnTiS or ZnCrS heterocluster could be a great semiconductor material for many uses.

In addition, the overlap between molecular orbitals plays a key role in understanding how charge moves between molecules. This includes calculating the overlap between the "highest occupied molecular orbitals (HOMO)" and the "lowest unoccupied molecular orbitals (LUMO)" in the H/OH group and the ZnS, ZnTiS or ZnCrS heterocluster. The calculation uses the "CAM-B3LYP-D3/6-311+G (d,p)" wavefunction level, which is used to determine the HOMO and LUMO values, respectively (see Table 2).

Table 2. Stability energy (kcal/mol), dipole moment (debye), LUMO (eV), HOMO (eV), and energy gap (ΔE) (eV) for heteroclusters of bare ZnS, ZnS (H^+OH^-), ZnTiS, ZnTiS (H^+OH^-), ZnCrS and ZnCrS (H^+OH^-)

Compounds	$E_{ads} \times 10^{-3}$ (kcal/mol)	D (debye)	E_{HOMO} (eV)	E_{LUMO} (eV)	$\Delta E = E_{LUMO} - E_{HOMO}$ (eV)
ZnS	-640.0751	0.0002	–2.7413	–1.1723	1.5690
ZnS (H^+OH^-)	-687.0415	0.5938	–2.7459	–1.1762	1.5697
ZnTiS	-635.4318	1.9668	-2.2415	-1.6605	0.5810
ZnTiS (H^+OH^-)	-682.4344	6.2397	-3.1906	-1.7641	1.4265
ZnCrS	-653.4013	3.6606	-2.6340	-1.6236	1.0104
ZnCrS (H^+OH^-)	-700.4265	3.9229	-2.7738	-1.7509	1.0229

Doping of transition metal ions in ZnO crystal lattice is a good technique to improve its activity as the dopant metals create new energy levels in the band gap which primarily improve the charge separation efficiency of e^-/h^+ by forming electron traps. As Ti and Cr doped on the ZnS surface, their shape and electric charge arrangement undergo a significant change. This phenomenon is enhanced by the presence of a metal atom such as Ti or Cr on the ZnS surface, which increases the polarity of the hybrid complexes (Table 2).

As water molecules approach the surface, their shape and electric charge arrangement undergo a significant change. This phenomenon is enhanced by the presence of a metal atom such as titanium or chromium on the ZnS surface, which increases the polarity of water molecules. Consequently, the electric charge arrangement of water molecules at the surface is more pronounced compared to when they are isolated (Fig. 5).

Comparing the undoped ZnS nanoparticles and the Cr-doped ZnS nanoparticles in Fig. 5 showed that Cr ions replaced Zn ions effectively.

The "Mayer bond" order (Mayer, 2012) is usually close to 1.0 for a single bond, based on empirical bond order. The "Mulliken bond" (Singh and Yadav, 1987) order only slightly matches the empirical bond order and isn't a good way to measure bonding strength, as Mayer bond order is better for that. However, "Mulliken bond" order is still useful as a qualitative tool to show whether bonding or

antibonding is present, with positive values showing bonding and negative values showing antibonding (Table 3).

As shown in Table 3, "Laplacian bond order" (Lu and Chen, 2013) shows a direct relationship with "bond polarity", "bond dissociation energy", and "bond vibrational frequency". The low value of "Laplacian bond order" suggests that it is not very sensitive to the level of calculation used to generate electron density. Generally, the value of "Fuzzy bond order" is close to "Mayer bond order", especially for less polar bonds, but it is more consistent when there are changes in the basis set. Calculating "Fuzzy bond order" requires running "Becke's DFT numerical integration", which leads to a higher value compared to "Mayer bond order" and provides a more accurate assessment (Visavakitcharoen et al., 2023; Wang et al., 2024).

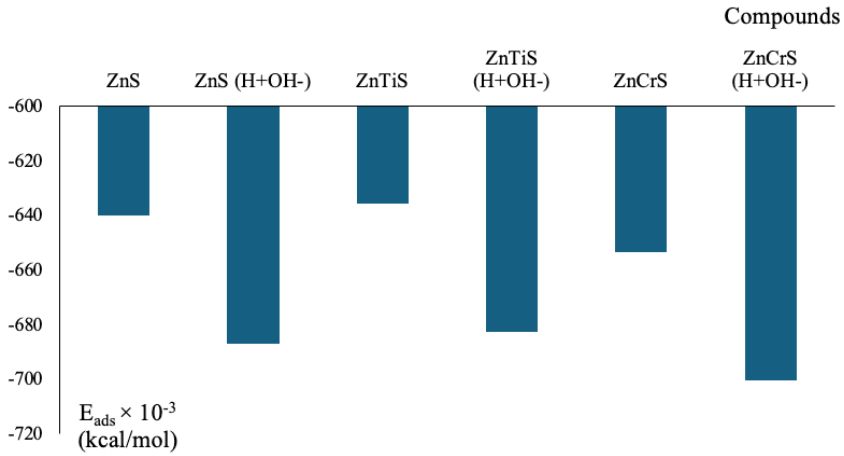

Fig. 5. Stability energy (kcal/mol) for heteroclusters of bare ZnS, ZnS (H^+OH^-), ZnTiS, ZnTiS (H^+OH^-), ZnCrS and ZnCrS (H^+OH^-)

Table 3. The bond order of "Mayer", "Wiberg", "Mulliken", "Laplacian" and "Fuzzy" from "mixed alpha and beta density matrix" for ZnS, ZnTiS or ZnCrS heterocluster through "H/OH adsorption" and formation of hydrated ZnS (H^+OH^-), ZnTiS (H^+OH^-) or ZnCrS (H^+OH^-) heterocluster

Bond order	Hydrated ZnS			Hydrated ZnTiS			Hydrated ZnCrS		
	O1–Zn15	O1–H29	S27–H30	O1–Ti15	O1–H29	S27–H30	O1–Cr15	O1–H29	S27–H30
Mayer	1.2782	0.6905	0.8056	2.1637	0.3121	0.5799	1.7305	0.4968	0.7456
Wiberg	1.0554	0.6397	0.6436	1.9586	0.4188	0.5812	1.5234	0.5232	0.6172
Mulliken	1.8753	0.1573	0.1864	1.9951	0.1702	0.183	1.8319	0.1719	0.1401
Laplacian	1.7453	0.2014	0.2491	2.142378	0.156486	0.190334	1.6548	0.2092	0.1891
Fuzzy	1.5246	0.6273	0.6852	2.1745	0.4786	0.6571	1.8433	0.5626	0.6781

4. Conclusions

A lot of focus has been placed recently on bare ZnS, ZnTiS or ZnCrS as a material with many useful functions and a variety of technology uses. It's important to understand how water interacts with bare ZnS, ZnTiS or ZnCrS because this knowledge is crucial for using the material in areas like gas sensing, catalysis, and biomedical uses. In short, we looked into how H_2O binds to bare ZnS, ZnTiS or ZnCrS using first-principles calculations. We started by creating a bare ZnS, ZnTiS or ZnCrS heterocluster and then studied the geometric features of H and OH adsorption on the ZnS, ZnTiS or ZnCrS surface by looking at how the atoms absorb and how electron density changes. The hydrated ZnS (H^+OH^-), ZnTiS (H^+OH^-) or ZnCrS (H^+OH^-) heterocluster shows a bigger electron delocalization area because of the labeled atoms "O1, Zn15/Ti15/Cr15, O27, H29, and H30". As H^+OH^- ions approach the surface, their shape and electric charge arrangement undergo a significant change. This phenomenon is enhanced by the presence of a metal atom such as titanium or chromium on the ZnS surface, which increases the

polarity of the H^+OH^- ions. Consequently, the electric charge arrangement of H^+OH^- ions at the surface is more pronounced compared to when they are isolated.

Acknowledgments

In successfully completing this paper and its research, the author is grateful to Kastamonu University.

References

WANG, G., HUANG, B., LI, Z., LOU, Z., WANG, Z., DAI, Y., WHANGBO, M.-H., 2015, *Synthesis and characterization of ZnS with controlled amount of S vacancies for photocatalytic H_2 production under visible light*, Scientific Reports, 5, 8544.

KHAN, A.U., TAHIR, K., ALBALAWI, K. et al., 2022, *Materials Chemistry and Physics*, 291, 126667.

ZAGORAC, D., ZAGORAC, J., PEJIĆ, M., MATOVIĆ, B., SCHÖN, J.C., 2022, *Band Gap Engineering of Newly Discovered ZnO/ZnS Polytypic Nanomaterials*, Nanomaterials, 12, 1595.

DE MORAES, N.P., MARINS, L.G.P., DE MOURA YAMANAKA, M.Y., BACANI, R., DA SILVA ROCHA, R., RODRIGUES, L.A., 2021, *Efficient photodegradation of 4-chlorophenol under solar radiation using a new ZnO/ZnS/carbon xerogel composite as a photocatalyst*, Journal of Photochemistry and Photobiology A: Chemistry, 418, 113377.

BOLATOV, A., MANJOVELO, A., CHOUCHENE, B., BALAN, L., GRIES, T., MEDJAHDI, G., URALBEKOV, B., SCHNEIDER, R., 2024, *Ternary ZnS/ZnO/Graphitic Carbon Nitride Heterojunction for Photocatalytic Hydrogen Production*, Materials, 17, 4877.

DONG, Z., WU, Y., THIRUGNANAM, N., 2018, *Double Z-scheme ZnO/ZnS/g-C_3N_4 ternary structure for efficient photocatalytic H_2 production*, Applied Surface Science, 430, 293–300.

ZHANG, H., RUSTAD, J.R., BANFIELD, J.F., 2007, *Interaction between water molecules and zinc sulfide nanoparticles studied by temperature-programmed desorption and molecular dynamics simulations*, The Journal of Physical Chemistry A, 111, 5008–5014.

RAHMANI, R., LYUBARTSEV, A.P., 2023, *Biomolecular Adsorption at ZnS Nanomaterials: A Molecular Dynamics Simulation Study of the Adsorption Preferences, Effects of the Surface Curvature and Coating*, Nanomaterials, 13, 2239.

CHANG, Y.-C., CHEN, T.-J., LU, M.-Y., 2025, *Indium-doped zinc sulfide nanopowders for boosting photocatalytic stream water splitting*, Journal of Alloys and Compounds, 1012, 178464.

BHARGAVA, R.N., GALLAGHER, D., HONG, X., NURMIKKO, A.J.P.R.L., 1994, *Optical properties of manganese-doped nanocrystals of ZnS*, Physical Review Letters, 72(3), 416–418.

CHOI, H.-J., SEONG, H.-K., CHANG, J., LEE, K.-I., PARK, Y.-J., KIM, J.-J., LEE, S.-K., HE, R., KUYKENDALL, T., YANG, P., 2005, *Single-crystalline diluted magnetic semiconductor GaN: Mn nanowires*, Advanced Materials, 17(11), 1351–1356.

RADOVANOVIC, P.V., BARRELET, C.J., GRADECAK, S., QIAN, F., LIEBER, C.M., 2005, *General synthesis of manganese-doped II–VI and III–V semiconductor nanowires*, Nano Letters, 5(7), 1407–1411.

YATSUNENKO, S., ŚWIĄTEK, K., GODLEWSKI, M., FRÖBA, M., KLAR, P.J., HEIMBRODT, W., 2008, *Electron spin resonance investigations of ZnMnS nanoparticles*, Optical Materials, 30(5), 753–755.

KUDO, A., SEKIZAWA, M., 2000, *Photocatalytic H_2 evolution under visible light irradiation on Ni-doped ZnS photocatalyst*, Chemical Communications, 15, 1371–1372.

TSUJI, I., KUDO, A., 2003, *H_2 evolution from aqueous sulfite solutions under visible-light irradiation over Pb and halogen-codoped ZnS photocatalysts*, Journal of Photochemistry and Photobiology A: Chemistry, 156(1–3), 249–252.

KIPTARUS, J.J., KORIR, K.K., GITHINJI, D.N., KIRIAMITI, H.K., 2024, *A Review of Design and Development of Selected Transitional Metal Doped Zinc Sulphide Nanostructure Surface Layers Decorated with Graphene for Hydrogen Production*, International Journal of Materials Engineering, 14(1), 12–24.

CHAURASIYA, R., DIXIT, A., 2019, *Transition metal doped ZnS monolayer: the first principles insights*, The Physics of Semiconductor Devices: Proceedings of IWPSD 2017, 49–56.

CHEN, H.X., SHI, D.N., QI, J.S., WANG, B.L., 2011, *First-principles study on the magnetic properties of transition-metal atoms doped $(ZnS)_{12}$ cluster*, Journal of Magnetism and Magnetic Materials, 323, 781–785.

ALHASSAN, S.S., ABDULSALAM, M., 2024, *A DFT+U Study of the Structural and Electronic Properties of Zinc-Doped Anatase TiO_2 Nanomaterial*, UMYU Scientifica, 3(1), 186–191.

APOSTOLOVA, I., APOSTOLOV, A., WESSELINOWA, J., 2023, *Magnetic, Phonon and Optical Properties of Transition Metal and Rare Earth Ion Doped ZnS Nanoparticles*, Nanomaterials, 13, 79.

KOHN, W., SHAM, L.J., 1965, *Self-Consistent Equations Including Exchange and Correlation Effects*, Physical Review, 140, A1133–A1138.

BECKE, A.D., 1993, *Density-functional thermochemistry. III. The role of exact exchange*, Journal of Chemical Physics, 98(7), 5648–5652.

LEE, C., YANG, W., PARR, R.G., 1988, *Development of the Colle–Salvetti correlation-energy formula into a functional of the electron density*, Physical Review B, 37, 785–789.

MOLLAAMIN, F., MONAJJEMI, M., 2023, *Doping of Graphene Nanostructure with Iron, Nickel and Zinc as Selective Detector for the Toxic Gas Removal: A Density Functional Theory Study*, C, 9, 20.

MOLLAAMIN, F., MONAJJEMI, M., 2023, *Graphene-based resistant sensor decorated with Mn, Co, Cu for nitric oxide detection: Langmuir adsorption & DFT method*, Sensor Review, 43(4), 266–279.

MOLLAAMIN, F., 2024, *Competitive Intracellular Hydrogen-Nanocarrier Among Aluminum, Carbon, or Silicon Implantation: a Novel Technology of Eco-Friendly Energy Storage using Research Density Functional Theory*, Russian Journal of Physical Chemistry B, 18, 805–820.

MOLLAAMIN, F., 2014, *Features of parametric point nuclear magnetic resonance of metals implantation on boron nitride nanotube by density functional theory/electron paramagnetic resonance*, Journal of Computational and Theoretical Nanoscience, 11(11), 2393–2398.

FRISCH, M.J., TRUCKS, G.W., SCHLEGEL, H.B., SCUSERIA, G.E., ROBB, M.A. et al., 2016, *Gaussian 16, Revision C.01*, Gaussian Inc., Wallingford, CT.

DENNINGTON, R., KEITH, T.A., MILLAM, J.M., 2016, *GaussView, Version 6.06.16*, Semichem Inc., Shawnee Mission, KS.

XU, Z., QIN, C., YU, Y., JIANG, G., ZHAO, L., 2024, *First-principles study of adsorption, dissociation, and diffusion of hydrogen on a-U (110) surface*, AIP Advances, 14, 055114.

LU, T., CHEN, F., 2012, *Multiwfn: A multifunctional wavefunction analyzer*, Journal of Computational Chemistry, 33, 580–592.

LU, T., 2024, *A comprehensive electron wavefunction analysis toolbox for chemists, Multiwfn*, Journal of Chemical Physics, 161, 082503.

MURRAY, J.S., RILEY, K.E., BRINCK, T., 2024, *A Revival of Molecular Surface Electrostatic Potential Statistical Quantities: Ionic Solids and Liquids*, Crystals, 14, 995.

MAYER, I., 2012, *Improved definition of bond orders for correlated wave functions*, Chemical Physics Letters, 544, 83–86.

SINGH, O.P., YADAV, J.S., 1987, *Bond orders and valence indices: Relations to Mulliken's population analysis and covalent chemical reactivity*, Journal of Molecular Structure: THEOCHEM, 149(1–2), 91–96.

LU, T., CHEN, F., 2013, *Bond Order Analysis Based on the Laplacian of Electron Density in Fuzzy Overlap Space*, Journal of Physical Chemistry A, 117(14), 3100–3108.

VISAVAKITCHAROEN, A., ASSAWINCHAICHOTE, W., SHI, Y., ANGELI, C., 2023, *Event-triggered fuzzy integral control for a class of nonlinear singularly perturbed systems*, ISA Transactions, 139, 71–85.

WANG, X., ZHANG, X., PEDRYCZ, W., YANG, S.-H., BOUTAT, D., 2024, *Consensus of T-S Fuzzy Fractional-Order, Singular Perturbation, Multi-Agent Systems*, Fractal and Fractional, 8, 523.